Resonant tunneling of Bose-Einstein condensates in optical lattices

Alessandro Zenesini[†], Carlo Sias[∗], Hans Lignier[∗], Yeshpal Singh, Donatella Ciampini[†], Oliver Morsch[∗], Riccardo Mannella[†], Ennio Arimondo[∗,†]

Dipartimento di Fisica Enrico Fermi, Università degli Studi di Pisa, Largo Pontecorvo 3, I-56127 Pisa
[∗]CNR-INFM, Largo Pontecorvo 3, I-56127 Pisa
[†]CNISM Unitá di Pisa, Largo Pontecorvo 3, I-56127 Pisa

Andrea Tomadin

Scuola Normale Superiore, Piazza dei Cavalieri 7, I-56126 Pisa

Sandro Wimberger

Institut für Theoretische Physik, Universität Heidelberg, Philosophenweg 19, D-69120 Heidelberg

Abstract. In this article, we present theoretical as well as experimental results on resonantly enhanced tunneling of Bose-Einstein condensates in optical lattices both in the linear case and for small nonlinearities. Our results demonstrate the usefulness of condensates in optical lattices for simulating Hamiltonians originally used for describing solid state phenomena.

1. Introduction

In the last decade, the experimental techniques used in atom and quantum optics have made it possible to control the external and internal degrees of freedoms of ultracold atoms with a very high degree of precision. Thus, ultracold bosons or fermions loaded into optical lattices are optimal realizations of lattice models proposed and studied in the context of solid-state physics. Bose-Einstein condensates, for instance, have been used to simulate phenomena such as Bloch oscillations in tilted periodic potentials [1–6] and to study quantum phase transitions driven by atom-atom interactions [7].

Up to now most of the quantum transport phenomena investigated with Bose-Einstein condensates within periodic optical lattices focused on the atomic motion in the ground state band of the periodic lattice. Only a few experiments examined the quantum transport associated with interband transitions "vertical" in the energy space.

Interband transitions were induced by additional electromagnetic fields, as in the case of the spectroscopy of Wannier-Stark levels [8], or by quantum tunneling between the bands. Tunneling between otherwise uncoupled energy bands occurs when the bands are coupled by an additional force, which can be a static Stark force (tilting the otherwise periodic lattice) [6], or also by strong atom-atom interactions as observed for fermions in [9] and discussed for bosons in [10]. The quantum tunneling between the ground and the first excited band is particularly pronounced in the presence of degeneracies of the single-well energy levels within the optical lattice leading to resonantly enhanced tunneling (RET). RET is a quantum effect in which the probability for tunneling of a particle between two potential wells is increased when the energies of the initial and final states of the process coincide. Owing to the fundamental nature of this effect and the practical interest [11], in the last few years much progress has been made in constructing solid state systems such as superlattices [12–15], quantum wells [16] and waveguide arrays [17] which enable the controlled observation of RET. RET has also been examined theoretically for ultracold atoms trapped in an optical lattice [18–21].

RET-like effects have been observed in a number of experiments to date. In ref. [22], resonant tunneling was observed for cold atoms trapped by an optical lattice when an applied magnetic field produced a Zeeman splitting of the energy levels. At certain values of the applied magnetic field, the states in the up-shifting and down-shifting energy levels were tuned into resonance with one another. This led to RET drastically altering the quantum dynamics of the system and producing a modulation of the magnetization and lifetime of the atoms trapped by the optical lattice. Resonant tunneling has been observed in a Mott insulator within an optical lattice, where a finite amount of energy given by the on-site interaction energy is required to create a particle-hole excitation [23]. Tunneling of the atoms is therefore suppressed. If the lattice potential is tilted by application of a potential gradient, RET is allowed whenever the energy difference between neighboring lattice sites due to the potential gradient matches the on-site interaction energy. The corresponding nonlinear effect in a Mott insulator allowed Fölling *et. al.* [24] to observe two-atom RET, and RET in the presence of many-body coherences was theoretically analyzed in [25]. We reported very precise RET measurements for Bose-Einstein condensates in [26]. The condensates were loaded into a one-dimensional optical lattice and subjected to an additional Stark force, optimally implemented and controlled by accelerating the lattice.

In this paper, we report additional investigations on RET for a Bose-Einstein condensate in a one-dimensional optical lattice applying the high-level control elaborated in our previous work. The experimental data presented here concentrates on the regime of parameters for which the Stark force dominates the dynamics of the condensate. Our precise control on the experimental parameters (lattice depth, interaction strength, and the flexibility on the choice of the initially populated band) enables us to measure the RET decay of the ground band and the first two excited energy bands in a wide range of experimental conditions. Moreover, we study the impact of atom-atom interactions on the RET process. All these features extend previous experimental studies on Landau-

Zener tunneling for ultracold atoms in periodic potentials [3, 4, 27, 28]. A theoretical description complements our experimental work.

The paper is organized as follows. Section 2.1 collects the necessary theoretical tools to describe our experiments, while section 2.2 introduces the RET modifications produced by the atom-atom interactions. Section 3.1 presents our experimental data in the linear tunneling regime, i.e., in the absence of atom-atom interactions. The effect of the latter is investigated in section 3.2, before we discuss and summarize our results in section 4.

2. Theoretical description

2.1. Single-particle RET

Neglecting for a moment atom-atom interactions in a Bose-Einstein condensate, our system is described by the following Hamiltonian:

$$H = -\frac{\hbar^2}{2M}\frac{d^2}{dx^2} + V_0 \sin^2\left(\frac{\pi x}{d_L}\right) + Fx \ . \tag{1}$$

V_0 is the depth of the optical lattice, d_L its spatial period, and M the atomic mass of Rubidium 87. This Hamiltonian defines the well-known Wannier-Stark problem [19, 29, 30].

For small Stark forces F, one can picture the evolution of a momentum eigenstate induced by Eq. (1) as an oscillatory motion in the ground energy band of the periodic lattice. These Bloch oscillations with period $T_{\mathrm{Bloch}} = h/d_L F$, where h is Planck's constant, were observed for cold and ultracold atoms in optical lattices [6].

At stronger forces, a wave packet prepared in the ground-state band has a significant probability to tunnel at the band edge (where the band gap Δ is minimal) to the first excited band. For a single tunneling event, such a probability is best estimated by Landau-Zener theory as [30]

$$\mathrm{P_{LZ}} = e^{-\pi^2(\Delta/E_{\mathrm{rec}})^2/(8F_0)} \ , \tag{2}$$

with the recoil energy $E_{\mathrm{rec}} = (\hbar\pi/d_L)^2/2M$ and $F_0 \equiv Fd_L/E_{\mathrm{rec}}$. The decay rate – owing to a sequence of Landau-Zener tunneling events – is then obtained by multiplying $\mathrm{P_{LZ}}$ with the Bloch frequency [19]

$$\Gamma_{\mathrm{LZ}} = \nu_{\mathrm{rec}} F_0 e^{-\pi^2(\Delta/E_{\mathrm{rec}})^2/(8F_0)} \ , \tag{3}$$

where the recoil frequency is given by $\nu_{\mathrm{rec}} = E_{\mathrm{rec}}/\hbar$.

The actual decay rates can dramatically deviate from Eq. (3) when two Wannier-Stark levels in different potentials wells are strongly coupled owing to an accidental degeneracy. By imposing an energy resonance between the Wannier-Stark levels in different wells of an optical lattice shifted by the potential of the external force, one finds that these degeneracies occur at the values F at which $Fd_L\Delta i$ (Δi integer) is close to the mean band gap between two coupled bands of the $F = 0$ problem [15, 19].
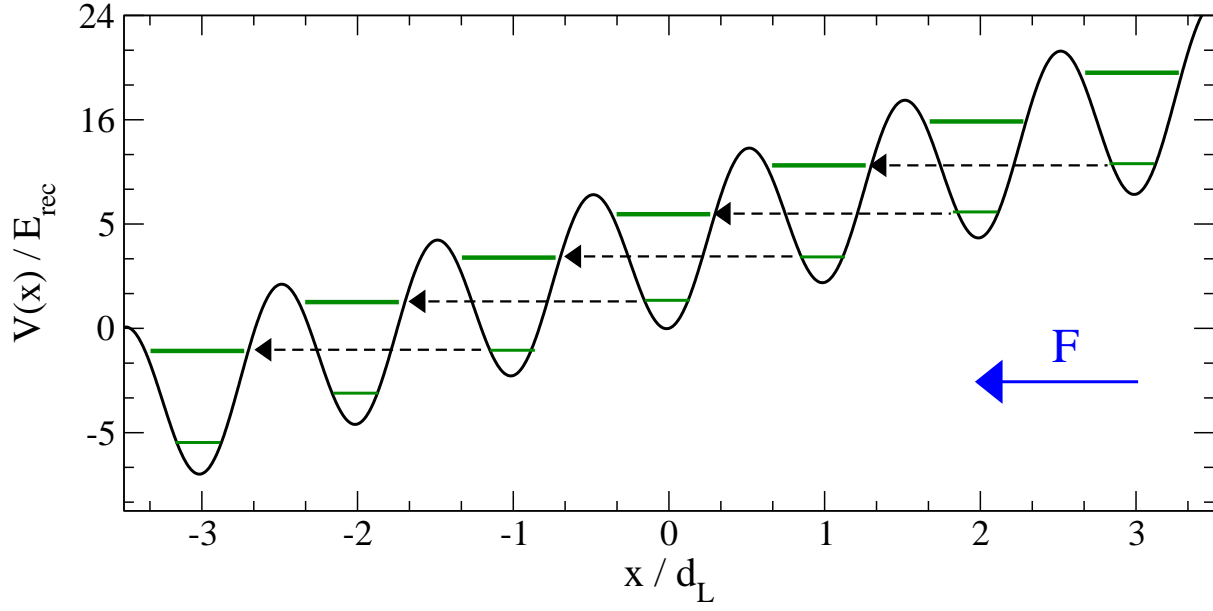
Figure 1. Schematic of the RET process between second nearest neighboring wells, i.e., for $\Delta i = 2$. The tunneling of atoms is resonantly enhanced when the energy difference between lattice wells matches the separation between the energy levels in different potential wells.
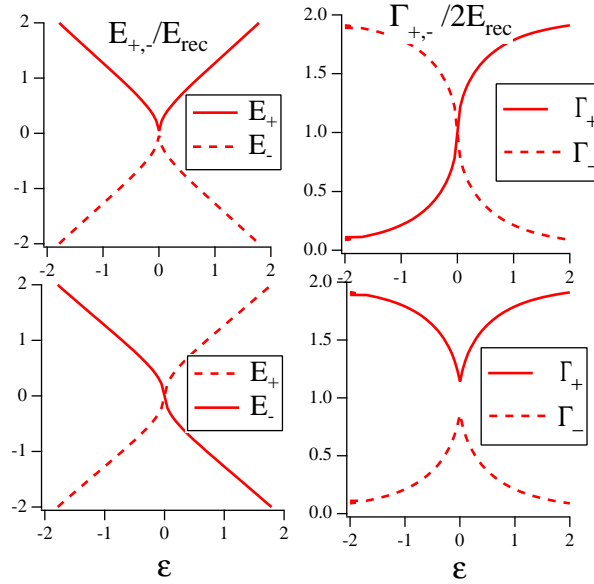

Figure 2. Real (left) and imaginary (right) part of the eigenvalues of Eq. (5) as a function of ϵ for $\gamma = 1$, measured in units of E_{rec}. A type-I crossing is found for $v = 1.01\, E_{\text{rec}}$ (upper plots), and a type-II crossing is found for $v = 0.99\, E_{\text{rec}}$ (lower plots).
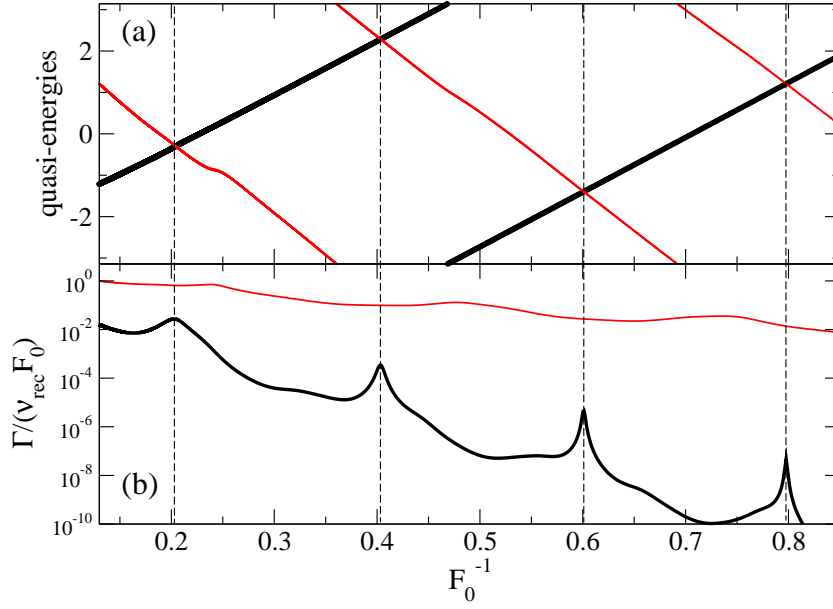
Figure 3. In (a) real part of the eigenenergies and in (b) decay rates for a lattice depth of $V_0/E_{\rm rec} = 10$ and the Hamiltonian from Eq. (1). The eigenenergies and the decay rates are associated with two Wannier-Stark ladders or, equivalently, with two energy bands: ground state (thick black lines) and first excited state (thin red lines). The maxima of the ground-state decay rates correspond to $\Delta i = 1, 2, 3$, and 4.

The actual peak positions are slightly shifted with respect to this simplified estimate, because the Wannier-Stark levels in the potential wells are only approximately defined by the averaged band gap of the $F = 0$ problem, a consequence of field-induced level shifts [19]. The RET process based on the $n = 1$ and $n = 2$ levels of the Wannier-Stark ladder is sketched in Fig. 1.

The modification of the level decay rate by the presence of a degeneracy may be described by a simple model of a two-level Hamiltonian with energy splitting 2ϵ and one decaying level [31, 32]

$$H = \begin{bmatrix} \epsilon - i\gamma & v \\ v & -\epsilon \end{bmatrix}. \tag{4}$$

In this approach it is assumed that the upper bare state decays with rate γ, while the decay is negligible for the other one. The two states are coupled with strength v. The eigenvalues of the non-hermitian Hamiltonian of Eq. 4 are given by

$$\mathcal{E}_\pm = -i\gamma \pm \sqrt{(\epsilon - i\gamma)^2 + v^2} = E_\pm - i\Gamma_\pm/2. \tag{5}$$

Real and imaginary part of the eigenvalues are different for $\epsilon \neq 0$, but crossings or anticrossings of the real and imaginary part are found at the critical value $\epsilon = 0$ where two different scenarios take place. For $|v| \geq \gamma$, at $\epsilon = 0$ the imaginary parts of the eigenvalues coincide, $\Gamma_+ = \Gamma_- = 2\gamma$, while the real parts differ. In this case, denoted as type-I crossing, the imaginary parts of the eigenvalues cross while the real parts anti-cross, as shown in the upper plots of Fig. 2. For $|v| \leq \gamma$, at $\epsilon = 0$ the real parts of

the eigenvalues coincide, $E_+ = E_- = 0$, while the imaginary parts differ. In this case, denoted as type-II crossing, the eigenvalues anticross while the real parts cross, as shown in the lower plots of Fig. 2. Type-II crossing corresponds to the RET phenomenon: if the lower state is energetically close or equal to the decaying upper level, the decay rate of the lower state increases significantly. In addition the upper state experiences a resonantly stabilized tunneling (RST) with a decrease of its decay rate.

For non-interacting atoms described by Eq. (1), we can easily diagonalize an opened version of our Hamiltonian [18,19,33,34,36] to obtain the true resonance eigenstates and eigenenergies of our decaying system. Fig. 3(a) shows the crossing and anticrossings for the real parts of the eigenenergies associated with a configuration investigated experimentally as a function of the experimental control parameter, the Stark force. It may be noticed that type-II crossings are typically encountered for our problem of decay from lower bands. The associated Wannier-Stark states decay with rates are shown in Fig. 3(b) as a function of the dimensionless parameter F_0. The strong modulations on top of the global exponential decrease arise from RET processes originated by the type-II crossings.

2.2. Interacting Bose-Einstein condensate dynamics

In this section we discuss the effect of atom-atom interactions in the Bose-Einstein condensate and how to effectively model them for a quantitative description of the experiment. We focus on a parameter regime where the Stark force essentially dominates the dynamics of the condensate. Here the quantum tunneling between the energy bands is significant and most easily detected experimentally. The critical field values for which such excitations are relevant can be estimated by comparing, for instance, the potential energy difference between neighboring wells, Fd_L, with the coupling parameters of the many-body Bose-Hubbard model, i.e., the hopping constant J and interaction constant U [6]. These parameters are plotted in Fig. 4 for typical experimental parameters as a function of the lattice depth V_0.

Our theoretical and experimental analysis will exclude the regime of $F_0 \leq J/E_\mathrm{rec}$ where a quantum chaotic system is realized [37–40]. The origin of quantum chaos, i.e., of the strongly force-dependent, nonperturbative mixing of energy levels can be understood as a consequence of the interaction-induced lifting of the degeneracy of the multiparticle Wannier-Stark levels in the crossover regime from Bloch to Wannier spectra, making nearby levels strongly interact, for comparable magnitudes of hopping matrix elements and Stark shifts.

For the regime of $F_0 \gg J/E_\mathrm{rec}$ studied here, the effect of weak interactions is just a perturbative shifting and a small splitting of many-body energy levels [33, 40]. As a consequence, we can use a global mean-field description based on the Gross-Pitaevskii equation [41] to simulate the temporal evolution of a Bose-Einstein condensate wave function $\psi(\vec{r}, t)$ subjected to a realistic potential
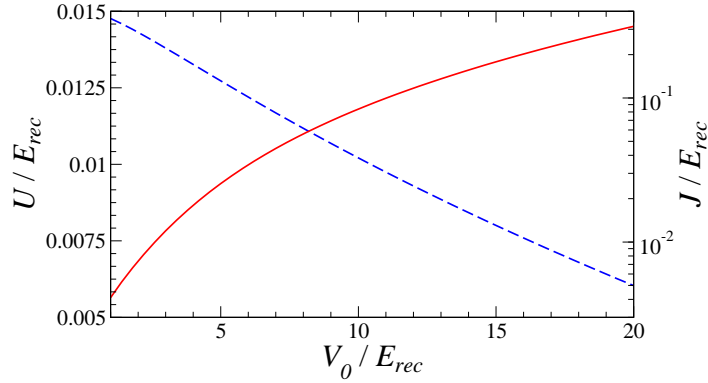
Figure 4. Hopping parameter J (dashed line) and on-site interaction constant U (solid line) of a 1D Bose-Hubbard model as a function of the depth of the optical lattice. U is computed for Rubidium 87 and for typical experimental parameters, i.e., lattice spacing $d_L = 620\,$nm, and radial confinement frequency $\omega_r/2\pi = 250\,$Hz, using the projection to a quasi-1D situation of [42].

.

$$i\hbar\frac{\partial}{\partial t}\psi(\vec{r},t) =$$
$$\left[-\frac{\hbar^2}{2M}\nabla^2 + \frac{1}{2}M\left(\omega_x^2 x^2 + \omega_r^2\rho^2\right) + V_0\sin^2\left(\frac{\pi x}{d_L}\right) + Fx + g\,|\psi(\vec{r},t)|^2\right]\psi(\vec{r},t). \quad (6)$$

The frequencies ω_x and ω_r characterize the longitudinal and transverse harmonic confinement (with cylindrical symmetry of the optical dipole trap: $\rho = \sqrt{y^2 + z^2}$, cf. section 3). The atom-atom interactions are modeled by the nonlinear term in Eq. (6),with the nonlinear coupling constant given by $g = 4\pi\hbar^2 a_s/M$, where a_s is the s-wave scattering length [41]. Later, we will use the dimensionless nonlinearity parameter $C = gn_0/(8E_{\rm rec})$ [4, 6], which is computed from the peak density n_0 of the initial state of the condensate, to describe the experimentally relevant nonlinear couplings $C \approx 0.01\ldots0.06$. In the Thomas-Fermi regime of the condensate [41], for given ω_x and ω_r the density n, and therefore C, is proportional to $N^{2/5}$ where N is the number of atoms in the condensate.

The Gross-Pitaevskii equation (6) is numerically integrated using finite difference propagation, amended by predictor-corrector loops to reliably evolve the nonlinear interaction term [43]. To avoid any spurious effects owing to the fast spreading of the wave functions, we use a large numerical basis, especially in the longitudinal direction. In this way, we fully cover the 3D expansion of the entire wave packet, including its tunneled tail, without the use of non-Hermitian potentials. The initial state propagated by Eq. (6) is the relaxed condensate wave function, adiabatically loaded into the confining potential given by the harmonic trap and the optical lattice (at $F = 0$).

In oder to have access to the decay rates in the experiment, one needs to measure the temporal evolution of the probability of the condensate to remain in the energy band, in which it has been prepared initially. As proposed in [21], such a survival

probability is best measured in momentum space, since, experimentally, the most easily measurable quantity is the momentum distribution of the condensate obtained from a free expansion after the evolution inside the lattice. From the momentum distributions we determine the survival probability by projection of the evolved state $\psi(\vec{p}, t)$ onto the support of the initial state:

$$P_{\text{sur}}(t) \equiv \int_{-p_c}^{p_c} dp_x \left(\int dp_y dp_z |\psi(\vec{p}, t)|^2 \right) . \tag{7}$$

A good choice is $p_c \geq 3p_R$ since typically three momentum peaks are initially significantly populated when loading the condensate adiabatically into the periodic lattice, and they correspond to $-2p_R, 0, 2p_R$ [3, 4, 6]. For $g = 0$, the individual tunneling events occurring when the condensate crossed the band edge are independent, and hence $P_{\text{sur}}(t)$ has a purely exponential form (apart from the $t \to 0$ limit [44]). When the nonlinear interaction term is present, the density decays with time too. As a consequence, the rates Γ are at best defined locally in time, and in the presence of RET even a sharp non-exponential decay is possible, as discussed in [35, 36]. Nevertheless, for the short evolution times and the weak nonlinear coupling strengths C that are experimentally accessible, the decay of the condensate can be well fitted by an exponential law [26, 45]

$$P_{\text{sur}}(t) = P_{\text{sur}}(t = 0) \exp(-\Gamma_n t) = \exp(-\Gamma_n t) , \tag{8}$$

with rates Γ_n for the band $n = 1$ (ground band), 2 (first excited band), 3 (second excited band), in which the atoms are initially prepared.

Before we discuss our experimental setup and present our data on linear and nonlinear tunneling, we come back to the RET peaks discussed above, c.f., Fig. 1. These peaks, which are predicted to occur for the single-particle motion studied in section 2.1, will be affected by the nonlinear interaction term of Eq. (6). A shift of the RET peaks in energy or in the position of the Stark force, as predicted in [33] for much larger parameters C, is negligible for our nonlinearities $C < 0.06$, for which such a shift would correspond to the extremely small amount of $\Delta F_0 < 5 \times 10^{-4}$ [33]. The RET peaks, however, originate from an exact matching of energy levels in neighboring potential wells, and hence they are very sensitive to slight perturbations. We may estimate the necessary perturbation by the nonlinear term in Eq. (6) by comparing the width of the RET peaks of a band n (which essentially is determined by the decay width Γ_{n+1} of the band into which the atoms tunnel) with the energy scale of the nonlinearity. In the experiment we can easily reach nonlinearities corresponding to this order-of-magnitude argument, and the consequences will be discussed in section 3.2 below.

3. Experimental results

The starting point of the measurements presented in this article is the creation of a Bose-Einstein condensate (BEC) of ^{87}Rb atoms. This is realized starting from a cloud of

atoms trapped in a 3D magneto-optical trap (MOT) and then loaded in a pure-magnetic time-orbital potential (TOP) trap after a molasses stage for sub-Doppler cooling. In order to achieve condensation, evaporative cooling is performed first in the TOP trap and then in an all-optical dipolar trap, where the atoms are transferred once they have a temperature of few μK. A BEC of up to 5×10^4 atoms then forms in the optical trap. The dipolar trap is realized with two off-resonant Gaussian laser beams focused to waists of $50\,\mu$m, having a wavelength $\lambda = 1030$ nm, and mutually detuned by ~ 220 MHz in order to avoid interference. The aspect ratio of the trap can be varied through the power of the laser beams, which is up to 1 W each and actively controlled by a feed-back loop. This feedback loop permits us to decrease the intensity noise on the beams and to improve reproducibility during the data collection.

After the creation of the condensate, the trap frequencies are adiabatically varied in order to confine the BECs in a cigar-shaped trap, with a longitudinal frequency of ~ 20 Hz and radial frequency in the range $80 - 250$ Hz. The BECs are then loaded into a one-dimensional optical lattice oriented along the weak direction of the dipolar trap. The lattice is created by optical interference of two linearly polarized Gaussian laser beams ($\lambda = 852$ nm) focused to a waist of $120\,\mu$m and intersecting with an angle θ. The lattice spacing is then $d_L = \lambda/(2\sin(\theta/2))$. The lattice depth V_0 is controlled through the laser intensity, and will be expressed in units of the recoil energy $E_{\rm rec}$. The measurements presented in the article were taken for different values of the lattice depth and of the lattice spacing: $V_0/E_{rec} = 6, 4, 9, 16$ with $d_L = 0.426\mu m$, and $V_0/E_{rec} = 2.5, 10, 12, 14$ with $d_L = 0.620\,\mu$m. Each lattice beam passes through an acousto-optic modulator (AOM) in order to control its power and hence the lattice depth. Moreover, by varying the radio-frequency driving one of the two AOMs, it is possible to create a detuning $\Delta\nu$ between the two lattice beams. This causes a displacement in time of the lattice in the laboratory frame. Within this frame, it is possible to make the lattice move at a velocity $v = d_L\Delta\nu$, or to accelerate it with an acceleration $a = d_L(d\Delta\nu/dt)$.

The lattice is usually loaded in 1 ms to avoid excitations to higher bands, and the atoms occupy the fundamental band if they have zero group velocity in the lattice rest frame during the loading phase. However, if the lattice is loaded with a constant velocity, the atoms can occupy one of the excited bands if the energy and quasi-momentum are conserved [1]. Furthermore, when the lattice is accelerated, the atoms are subjected to a force $F = ma$ in the rest frame of the lattice: this corresponds to the experimental realization of the Hamiltonian (1). The applied force F is chosen in order to minimize the growth of dynamical instabilities, as explored in [46].

In order to measure the tunneling rate Γ_n for BECs initially loaded into the n-th band of the optical lattice (ground state: $n = 1$, first excited state: $n = 2$, etc.), the lattice is accelerated with acceleration a for an integer number of Bloch oscillation cycles. During this acceleration time, atoms are most likely to tunnel to upper bands when the condensate quasi-momentum is close to the edge of the Brillouin zone. Atoms that do not tunnel to a higher band and are, therefore, "dragged along" by the accelerated lattice acquire a larger final velocity than those that have undergone tunneling. They

are spatially separated from the latter by releasing the BEC from the dipole trap and lattice at the end of the acceleration period and allowing it to expand and to fall under gravity for $5 - 20$ ms. After the time-of-flight, the atoms are detected by absorptive imaging on a CCD camera using a resonant flash.

¿From the dragged fraction N_{drag}/N_{tot}, we then determine the tunneling rate Γ_n by imposing the asymptotic decay law

$$N_{drag}(t) = N_{tot} \exp\left(-\Gamma_n t\right) \tag{9}$$

where the subscript n indicates the dependence of the tunneling rate on the local energy level n in which the atoms are initially prepared. Our measurement of Γ_n based on the dragged fraction relies on the fact that for the lattice depths used in our experiments the number of bound states in the wells was small (2-4, depending on the lattice depth), so after the first tunneling event, the probability for tunneling to the next bound state or the continuum was close to unity. This explains why we observe type-II crossings, corresponding to $\gamma > |v|$ in the model discussed in section 2.1.

The way in which we measure the tunneling rate also determines the achievable resolution of our method. This is given by the minimum number of atoms that we can distinguish reliably from the background noise in our CCD images, which varies between 500 and 1000 atoms, depending on the width of the observed region. With our condensate number, and taking into account the minimum acceleration time limited by the need to spatially separate the two fractions after time-of-flight and the maximum acceleration time limited by the field of view of the CCD camera, this results in a maximum $\Gamma_n/\nu_{\rm rec}$ of ≈ 1 and a minimum of $\approx 1 \times 10^{-2}$.

3.1. The linear regime

Although the finite and positive scattering length of the 87-Rb atoms in our BECs means that the linear Hamiltonian of Eq.(1) is never exactly realized in our experiments, we can approximate a non-interacting BEC by keeping the condensate density low. In that case, the interaction energy can be made much smaller than all the other energy scales of the system (recoil energy, band width, gap width) and hence negligible for our purposes. A low density can be achieved by using a weak trap with small trap frequencies and/or a small atom number in the BEC. Alternatively, one can also allow the BEC to expand freely for a short time (typically less than a millisecond, to avoid excessive dropping under gravity) before performing the lattice acceleration.

Fig. 5 shows the results of experiments with low-density condensates for which the nonlinearity parameter C was less than $\approx 1 \times 10^{-2}$, which in this work we define to be the limit of the linear regime. In each plot, the tunneling rate Γ_n out of the n-th band (in our experiments we were able to study the cases $n = 1, 2$ and 3) is shown as a function of F_0^{-1}. Superimposed on the overall exponential decay of Γ_n/F_0 with F_0^{-1}, one clearly sees the resonant tunneling peaks corresponding to the various resonances $\Delta i = 1, 2, 3, 4$. Which of the resonances were visible in any given experiment depended on the choice of lattice parameters and the finite experimental resolution. The limit
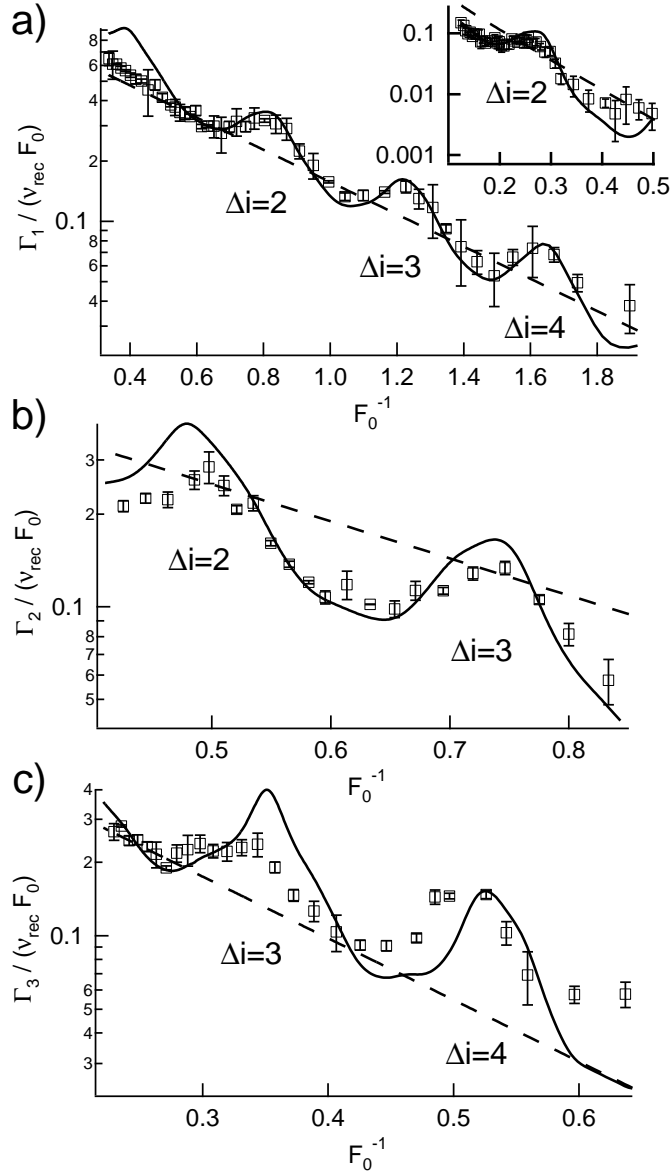
Figure 5. Resonant tunneling in the linear regime. Shown here are the tunneling rates from the three lowest energy bands of the lattice as a function of the normalized inverse force F_0^{-1} for lattice depths (a) $V_0/E_{\rm rec} = 2.45$ (insert: $V_0/E_{\rm rec} = 6$), (b) $V_0/E_{\rm rec} = 10$ and (c) $V_0/E_{\rm rec} = 23$. Note the different scales on the horizontal axes.

.

$n = 3$ for the highest band we could explore was given by the maximum lattice depth achievable.

The inset in Fig. 5 (a) shows the tunneling resonances in the lowest energy band for a different value of the lattice depth V_0. One clearly sees that the positions of the resonances are shifted according to the variation in the energy levels. Fig. 6 (a) shows the positions $F_0^{\rm res}$ of the $\Delta i = 1$ resonances as a function of the lattice depth. For deep enough lattices, these positions agree perfectly with the results of a numerical

simulation (see Fig. 6 (a)) and can also be approximately calculated by making a harmonic approximation in the lattice wells, which predicts a separation of the two lowest energy levels ($n = 1$ and $n = 2$) of

$$\Delta E_{2-1} = 2E_{\text{rec}}\sqrt{\frac{V_0}{E_{\text{rec}}}}. \tag{10}$$

The resonance condition $\Delta E_{2-1} = F^{\text{res}}d_L\Delta i$ can then be used to calculate the resonance position F^{res}. Our experimental results of Fig. 5 (a) are well fitted by this formula if the factor 2 in the expression for ΔE_{2-1} is replaced by ≈ 1.5. This discrepancy with the theoretical prediction is to be expected since the anharmonicity of the potential wells reduces the actual energy separation of the levels compared to the harmonic case. While we were not able to measure the tunneling resonances in two *different* bands for the *same* lattice depth, we could measure the resonances in one single band and compare our results with the theoretically predicted resonances in an adjacent band [26]. This allowed us to confirm that in our experiments a resonance peak in one band always coincided with an anti-peak or trough in the adjacent band, which agrees with our interpretation in terms of a type-II crossing (see section 2.1).

We also studied the dependence of the widths of the tunneling resonances on the lattice depth. Physically, this width is determined by the width of the state to which the atoms tunnel and hence should decrease with increasing lattice depth. For instance, for tunneling from the ground state band $n = 1$, the resonance width should reflect the width of the first excited band $n = 2$. Figure 6 shows the results of our measurements. For large lattice depths, the resonance width decreases as expected, whereas for shallow lattices the behaviour is more complicated. This is also reflected in the numerical simulations.

3.2. The nonlinear regime

In order to enter the regime for which $C \gtrsim 1 \times 10^{-2}$, we carry out the acceleration experiments in radially tighter traps (radial frequency $\gtrsim 100\,\text{Hz}$) and hence at larger condensate densities. Fig. 7 shows the $\Delta i = 2$ and $\Delta i = 3$ resonance peaks of the ground-state band ($n = 1$) for increasing values of C, starting from the linear case and going up to $C \approx 3 \times 10^{-2}$. As the nonlinearity increases, two effects occur. First, the overall (off-resonant) level of Γ_1 increases linearly with C. This is in agreement with our earlier experiments on nonlinear Landau-Zener tunneling [3, 28] and can be explained describing the condensate evolution within a nonlinearity-dependent effective potential $V_{\text{eff}} = V_0/(1 + 4C)$ [47]. Second, with increasing nonlinearity, the contrast of the RET peak is decreased and the peak eventually vanishes, as is also evident from the different on-resonance and off-resonance dependence of the tunneling rate as a function of the atom number N (and hence the nonlinearity), as seen in Fig. 7 (b). This is in agreement with the theoretical discussion of section 2.

As mentioned in section 2.2, the critical value of C for which the nonlinearity significantly affects the resonance peak should be given by the width of the resonance
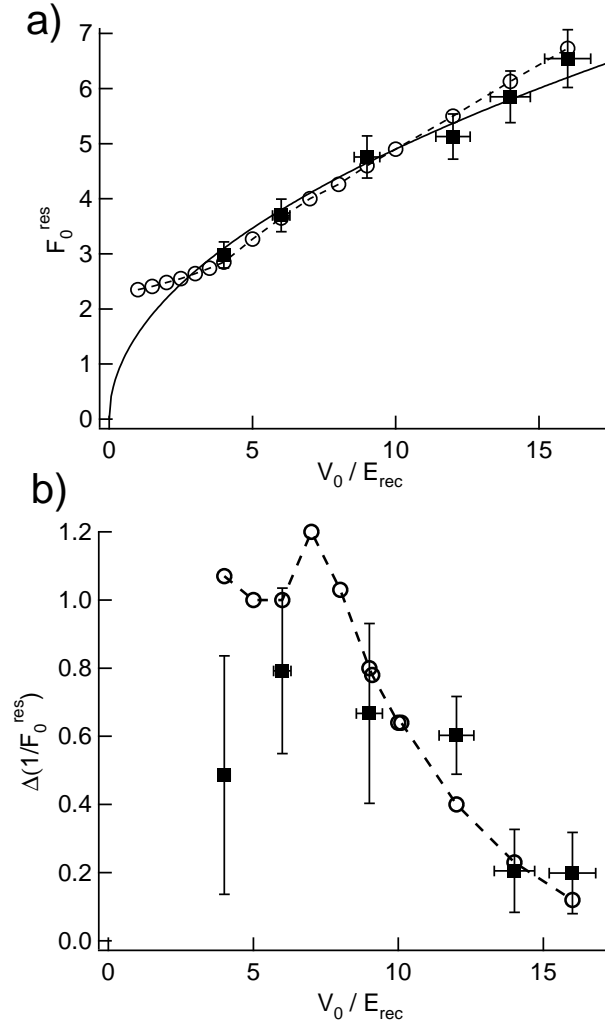
Figure 6. Positions (a) and widths (b) of the tunneling resonances with $\Delta i = 1$ in the lowest energy band as a function of the lattice depth. In (a), the dashed line is the theoretical prediction based on the harmonic oscillator approximation, modified as described in the main text. In (a) and (b), the open symbols connected by the dashed line are the results of a numerical simulation.

peak itself. For the parameters of Fig. 5 (a) and 7 (a) and the RET peak with $\Delta i = 2$, the typical width Γ_2 of the decaying state to which the atoms tunnel is of the order of $0.2 \ldots 0.5$, expressed in units of E_{rec}. Since C reflects the nonlinearity expressed in units of $8 \times E_{\text{rec}}$, this means that we expect to see substantial deviations from the linear behaviour when $C \gtrsim 0.025 \ldots 0.06$. Experimentally, we confirm that this threshold is a good estimate for the onset of the destruction of the RET peak, which is observed to occur around $C = 0.02$ in Fig. 7 (a).
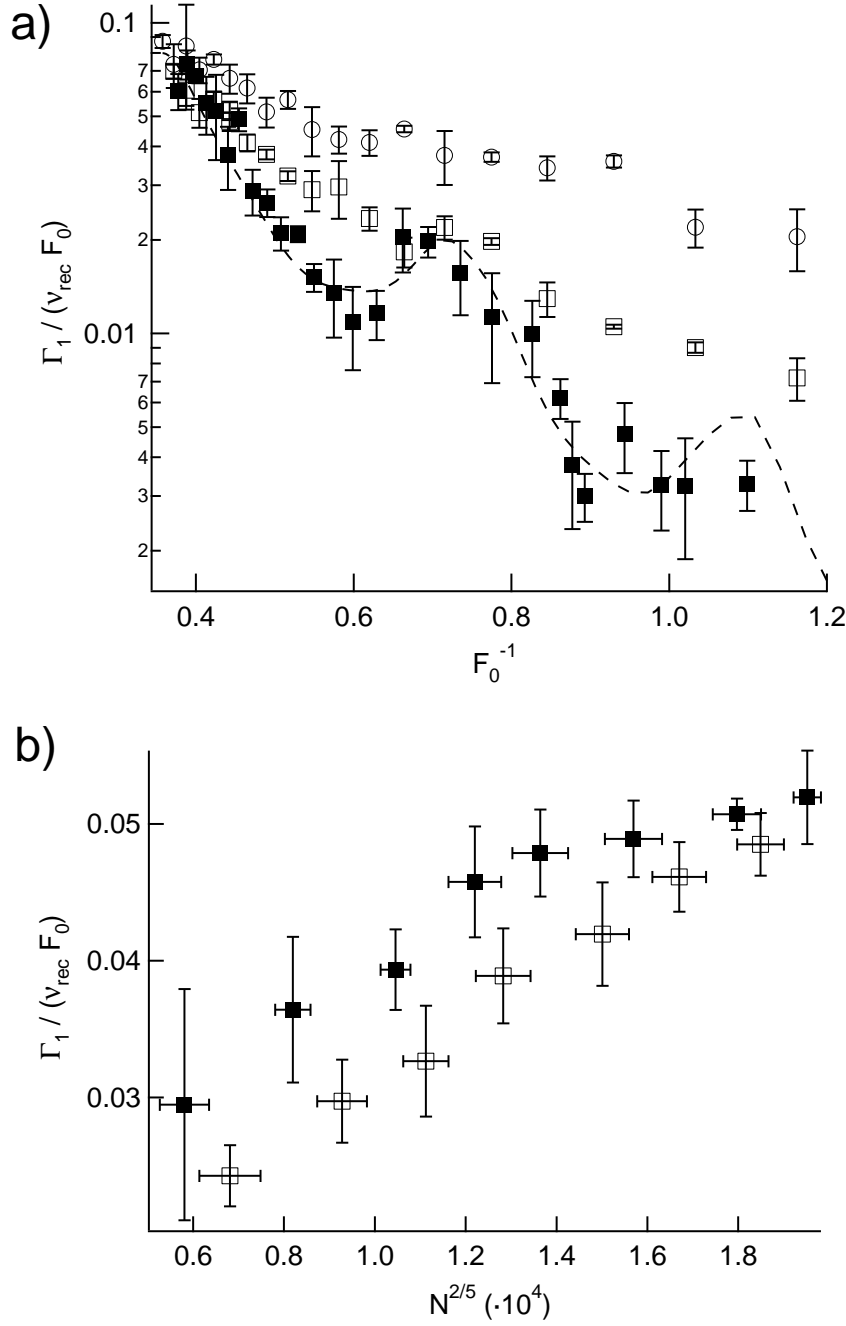
Figure 7. Resonant tunneling in the nonlinear regime. (a) The tunneling rates for $\Delta i = 2$ from the lowest energy band of the optical lattice as a function of the normalized inverse force F_0^{-1} for a lattice depth $V_0/E_{\rm rec} = 3.5$ and different values of $C \approx 0.01, 0.022, 0.033$ from bottom to top. The dashed line is the theoretical prediction in the linear regime. As the nonlinearity increases, the overall tunneling rate increases and the resonance peak becomes less pronounced. (b) Dependence on the condensate atom number N of the tunneling rate at the position of the peak $F_0^{-1} = 0.71$ (solid symbols) and of the through $F_0^{-1} = 0.60$ (open symbols) for $V_0/E_{\rm rec} = 3.0$.

.

4. Conclusions and outlook

In this paper, we have studied the resonantly enhanced tunneling of BECs in optical lattices both theoretically and experimentally. Our results show that ultracold atoms in periodic potentials are well suited to simulating and exploring basic quantum mechanical processes which are also the subject of active investigations in the solid state physics community, such as Bloch oscillations [48–51] and Zener tunneling [52, 53]. Compared to solid-state experiments, our approach offers the advantage of a large flexibility in the experimental parameters and the possibility to add a nonlinearity in a controlled way.

The experimental setup presented in this paper also opens up the possibility to explore different regimes, such as the strongly interacting regime for $J \simeq U \gtrsim F_0$ [39,40]. Another interesting aspect to be studied in the nonlinear regime is the limit in which the fraction of atoms undergoing tunneling is either very large (i.e., very few atoms remain in the initial band) or very small. In both limits, deviations from the the Gross-Pitaevskii equation, which presupposes a mean-field approximation for all the bands involved, are expected [54].

Acknowledgments

References

[1] BenDahan M, Peik E, Reichel J, Castin Y and Salomon C 1996 *Phys. Rev. Lett.* **76** 4508
[2] Raizen M, Salomon C and Niu Q 1997 *Phys. Today* **50** 30
[3] Morsch O, Müller JH, Cristiani M, Ciampini D and Arimondo E 2001 *Phys. Rev. Lett.* **87** 140402
[4] Cristiani M, Morsch O, Müller JH, Ciampini D and Arimondo E 2002 *Phys. Rev. A* **66** 02160
[5] Roati G, de Mirandes E, Ferlaino F, Ott H, Modugno G and Inguscio M 2004 *Phys. Rev. Lett.* **92** 230402
[6] Morsch O and Oberthaler M 2006 *Rev. Mod. Phys.* **78** 179
[7] Bloch I, Dalibard J and Zwerger W 2007 *Rev. Mod. Phys.* in press preprint arXiv:0704.3011
[8] Wilkinson S R, Bharucha C F, Madison K W, Niu Q and Raizen M G 1996 *Phys. Rev. Lett.* **76** 4512
[9] Köhl M, Moritz H, Stöferle T, Günter K and Esslinger T 2005 *Phys. Rev. Lett.* **94** 080403
[10] Lee C, Ostrovskaya E A and Kivshar 2007 *J. Phys. B: At. Mol. Opt. Phys.* **40** 4235
[11] Chang L L, Mendez E E, and Tejedor C (eds.) 1991 *Resonant Tunneling in Semiconductors* (Plenum, New York)
[12] Chang L L, Esaki L, and Tsu R 1974 *Appl. Phys. Lett.* **24** 593

[13] Esaki L 1986 *IEEE Journal Quant. Electr.* **QE-22(9)** 1611
[14] Leo K 2003 *High-Field Transport in Semiconductor Superlattices* (Springer, Berlin)
[15] Glutsch S 2004 Phys. Rev. B **69** 235317
[16] Wagner M and Mizuta H 1993 Phys. Rev. B **48** 14393 (1993)
[17] Rosam B, Leo K, Glück M, Keck F, Korsch H J, Zimmer F and Köhler K 2003 *Phys. Rev. B* **68** 125301
[18] Glück M, Kolovsky A R and Korsch H J 1999 *Phys. Rev. Lett.* **83** 891
[19] Glück M, Kolovsky A R and Korsch H J 2002 *Phys. Rep.* **366** 103
[20] Dounas-Frazer D R, Hermundstad A M and Carr L 2007 *Phys. Rev. Lett.* **99** 200402
[21] Wimberger S, Mannella R, Morsch O, Arimondo E, Kolovsky AR and Buchleitner A 2005 *Phys. Rev. A* **72** 063610
[22] Teo B K, Guest J R and Raithel G 2002 *Phys. Rev. Lett.* **88** 173001
[23] Greiner M, Mandel O, Esslinger T, Hänsch T W and Bloch I 2002 *Nature* **415** 39
[24] Fölling S, Trotzky S, Cheinet P, Feld M, Saers R, Widera A, Müller T and Bloch I 2007 *Nature* **448** 1029
[25] Lee C, Fu L B and Kivshar Y S 2008 *Europhys. Lett.* **81** 60006
[26] Sias C, Zenesini A, Lignier H, Wimberger S, Ciampini C, Morsch O and Arimondo E 2007 *Phys. Rev. Lett.* **98** 120403
[27] Bharucha C F, Madison K W, Morrow P R, Wilkinson S R, Sundaram B and Raizen M G 1997 *Phys. Rev. A* **55** R857
[28] Jona-Lasinio M, Morsch O, Cristiani M, Malossi N, Müller JH, Courtade E, Anderlini M and Arimondo E 2003 *Phys. Rev. Lett.* **91** 230406
[29] Nenciu G 1991 *Rev. Mod. Phys.* **63** 91
[30] Holthaus M 2000 *J. Opt. B* **2** 589
[31] Avron J E 1982 *Ann. Phys.* **143** 33
[32] Keck F, Korsch H-J and Mossmann S 2003 J. Phys. A **36** 2125
[33] Wimberger S, Schlagheck P and Mannella R 2006 *J. Phys. B: At. Mol. Opt. Phys.* **39** 729
[34] Witthaut D, Graefe E M, Wimberger S and Korsch H J 2007 *Phys. Rev. A* **75** 013617
[35] Carr L D, Holland M J and Malomed B A 2005 *J. Phys. B: At. Mol. Opt. Phys.* **38** 3217
[36] Schlagheck P and Wimberger S 2007 *Appl. Phys. B* **86** 385
[37] Buchleitner A and Kolovsky A R 2003 *Phys. Rev. Lett.* **91** 253002
[38] Thommen Q, Garreau JC and Zehnlé V 2003 *Phys. Rev. Lett.* **91** 210405
[39] Tomadin A, Mannella R and Wimberger R 2007 *Phys. Rev. Lett.* **98** 130402
[40] Tomadin A, Mannella R and Wimberger R 2008 *Phys. Rev. A* **77** 013606
[41] Pethick CJ and Smith H 2002 *Bose-Einstein Condensation in Dilute Gases* (Cambridge University Press, Cambridge)
    Pitaevskii L and Stringari S 2003 *Bose-Einstein Condensation* (Oxford University Press, Oxford)
[42] Bergeman T, Moore M G and Olshanii M 2003 *Phys. Rev. Lett.* **91** 16320
[43] Cerboneschi E, Mannella R, Arimondo E and Salasnich L 1998 *Phys. Lett. A* **249** 495
    Wimberger S, Mannella R, Morsch O and Arimondo E 2005 *Phys. Rev. Lett.* **94** 130404
[44] Wilkinson SR, Bharucha C F, Fischer M C, Madison K W, Morro P R, Niu Q, Sundaram B and Raizen M G 1997 *Nature* **387** 575
[45] Wimberger S, Ciampini C, Morsch O, Mannella R and Arimondo E 2007 *J. Phys. Conf. Ser.* **67** 012060
[46] Cristiani M, Morsch O, Malossi N, Jona-Lasinio M, Anderlini M, Courtade E and Arimondo E 2004 *Opt. Express* **12** 4
[47] Choi D I and Niu Q 1999 *Phys. Rev. Lett.* **82** 2022
[48] Feldmann J, Leo K, Shah J, Miller D A B, Cunningham J E, Meier T, von Plessen G, Schulze A, Thomas P and Schmitt-Rink S 1992 *Phys. Rev. B* **46** R7252
[49] Waschke C, Roskos H G, Schwedler R, Leo K, Kurz K and Köhler K 1993 *Phys. Rev. Lett.* **70** 3319

[50] Pertsch T, Dannberg P, Elflein W, Bräuer A and Lederer F 1999 *Phys. Rev. Lett.* **83** 4752

[51] Morandotti R, Peschel U, Aitchison J S, Eisenberg H S, Silberberg Y 1999 *Phys. Rev. Lett.* **83** 4756

[52] Ghulinyan M, Oton J C, Gaburro Z, Pavesi L, Toninelli C and Wiersma D S 2005 *Phys. Rev. Lett.* **94** 127401

[53] Trompeter H, Pertsch T, Lederer F, Michaelis D, Streppel U, Bräuer A and Peschel U 2006 *Phys. Rev. Lett.* **96** 023901

[54] Shchesnovich VS and Konotop VV 2007 *Phys. Rev. A* **75** 063628